Pattern with kinks and pulses in coupled periodic map lattices

Weiqing Liu,[1,2,3,4] Ye Wu,[1,2,3] Wei Zou,[1,2] Jinghua Xiao,[3] and Meng Zhan[1,*]
[1]*Wuhan Institute of Physics and Mathematics, Chinese Academy of Sciences, Wuhan 430071, China*
[2]*Graduate School of the Chinese Academy of Sciences, Beijing 100049, China*
[3]*School of Science, Beijing University of Posts and Telecommunications, Beijing 100876, China*
[4]*School of Science, Jiangxi University of Science and Technology, Ganzhou 341000, China*
(Received 2 February 2007; revised manuscript received 10 May 2007; published 27 September 2007)

In this paper, we reinvestigate the period doubling of kink-antikink patterns in coupled periodic logistic map lattices. In contrast to earlier observations, we find an additional mode structure, a pulse. An unusual brushlike bifurcation diagram and an oscillation of the largest Lyapunov exponent versus the coupling are observed. We propose a mode analysis method to analyze the cases of different mode numbers for these two basic modes (kink and pulse). We believe that our investigations can shed improved light on the dynamics of coupled periodic map lattices.

DOI: 10.1103/PhysRevE.76.036215 PACS number(s): 05.45.Ra, 05.45.Pq

I. INTRODUCTION

Most of the earlier studies [1] on nonlinear dynamics have concentrated on the temporal behavior of low-dimensional systems. However, a variety of physical systems of interest have many spatial degrees of freedom. Therefore, recent studies of spatiotemporal systems [2–12] have been central in nonlinear science and have received wide attention. One such system is the model of coupled map lattices (CMLs) [3–12], which serves as a paradigm for spatially extended nonlinear systems due to both its rich phenomenology and its computational efficiency.

In this paper, we investigate the standard one-dimensional diffusively coupled map lattice, written as

$$x_{n+1}(i) = (1-\varepsilon)f(x_n(i)) + \frac{\varepsilon}{2}[f(x_n(i-1)) + f(x_n(i+1))],$$

$$i = 1, \ldots, L, \tag{1}$$

where n is the discrete time step, i denotes the lattice site, and ε indicates the coupling intensity. Periodic boundary conditions are chosen throughout this paper. Without loss of generality, we take the logistic map for each lattice as $f(x) = \mu x(1-x)$ [13,14]. The dynamics of the single logistic map is well known. By increasing the nonlinear coefficient μ, the dynamics undergoes a period-doubling cascade and transits to chaos at the Feigenbaum accumulation point μ_∞ ($\mu_\infty = 3.569\,945\,6\ldots$). The first several period-doubling parameters are $\mu_{1\to 2}=3$ (for the $P1$ to $P2$ transition) and $\mu_{2\to 4} = 1+\sqrt{6} = 3.449\,41\ldots$ (for the $P2$ to $P4$ transition). Beyond μ_∞, multiband chaos appears and an inverse period-doubling cascade for the chaotic bands takes place, and at $\mu_r \approx 3.678$, two chaotic bands merge into a single-band chaotic state.

For coupled logistic map lattices [3–12], much richer phenomena have been found due to the mutual interactions of the local nonlinearity (μ) and the spatial coupling (ε), and several distinct patterns have been classified so far [3–7], including frozen random patterns, pattern selection, defect turbulence, pattern competition intermittency, fully developed turbulence, and so on. Below the value μ_r a frozen random pattern [5,8,10] appears, which is characterized by a system well separated by kink and antikinks (walls) into several isolated domains, in which the motions may be periodic or chaotic. As μ is decreased further, within the periodic parameter regime ($\mu_{1\to 2} < \mu < \mu_\infty$), the pattern gets simpler, characterized by flat regions and domain boundaries (kinks or antikinks). This has been termed period doubling of kink-antikink patterns [8]. Nevertheless, before the first period-doubling bifurcation point $\mu_{1\to 2}$, there is only one trivial homogeneous period-1 pattern available. In this regard, the pattern with kinks is the simplest but nontrivial complex pattern in coupled map lattices. Some important qualitative features have been addressed so far [8]: (1) The pattern is fixed in time; (2) if we start from a random initial condition, the pattern of the attractor is random in space and depends on the initial conditions; (3) the width of a kink is rather small and it increases as the coupling is increased. Obviously, a periodic pattern with kinks shares some essential properties with the frozen random pattern, which can be chaotic locally in some lattices, and may belong to the frozen random state, although it has also been viewed as an independent type of pattern with periodic behavior by some other researchers [11].

In the present work, we reinvestigate the period doubling of the kink-antikink pattern [8]. Our results show that, even for this simple pattern, previous observations are incomplete. A different type of mode, a pulse, is found. Both kink and pulse play constructive roles in the system's dynamical behavior. Furthermore, we develop a mode analysis method to characterize and even predict the pattern in a quantitative way.

II. NUMERICAL OBSERVATIONS

Let us consider $\mu = 3.1$ for a period-2 logistic map. In the absence of coupling ($\varepsilon = 0$), all lattices will converge to the stable period-2 states x_1^* and x_2^*, and alternate between them

*Author to whom correspondence should be addressed. zhanmeng@wipm.ac.cn

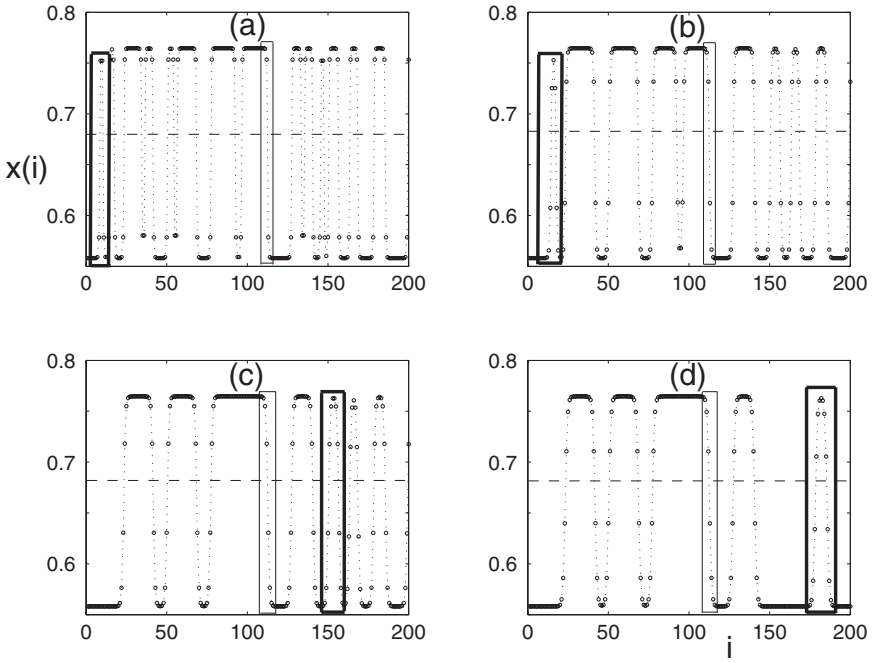

FIG. 1. Snapshots of the sites 1–200 of the CML ($L=1000$) under different couplings. Patterns emphasized in the thin rectangular boxes are kink patterns of different modes M_k and those in the heavy rectangular boxes are pulse patterns of different modes M_p. (a) $\varepsilon=0.03$, $(M_k, M_p)=(2,2)$. (b) $\varepsilon=0.085$, $(M_k, M_p)=(4,3)$. (c) $\varepsilon=0.14$, $(M_k, M_p)=(6,6)$. (d) $\varepsilon=0.20$, $(M_k, M_p)=(6,7)$.

in time. $x_1^*=[1+\mu-\sqrt{(\mu+1)(\mu-3)}]/2\mu$ and $x_2^*=[1+\mu+\sqrt{(\mu+1)(\mu-3)}]/2\mu$, which can be easily calculated. $x^*=1-1/\mu$ is the fixed point of the single logistic map and is unstable after $\mu_{1\to 2}=3$. $x_1^*\approx 0.558\ 01$, $x_2^*\approx 0.764\ 57$, and $x^*\approx 0.677\ 42$ for $\mu=3.1$ considered here. Figure 1 shows snapshots for different coupling strengths for the first 200 lattices only. $\varepsilon=0.03$, 0.085, 0.14, and 0.20 for Figs. 1(a)–1(d), respectively. $x=x^*$ is indicated by the dashed horizontal lines in the figures. The whole system size L is 1000 and all results are unchanged for any sufficiently large L. In Fig. 1, the parameter ε is adiabatically increased, by using the final configuration as the initial state for the subsequent simulation with ε increasing in steps of $\Delta\varepsilon=0.001$. Clearly the coupled system is well self-organized to a frozen random state with some flat regions (the original period-2 positions x_1^* and x_2^*) divided by domain boundaries (kinks). Here the word *frozen* means that all lattices switch to other positions in one time step and are unchanged at every second time step. The randomness of this pattern has also been well observed; we get different stable patterns for different initial conditions but the global structure and the detailed mode structures remain unchanged, as we will see. Both the flat regions and the boundaries (encircled by the thin rectangular boxes) get wider with the increase of ε; this finding is consistent with previous observations.

If we take a closer look at these patterns, surprisingly some unusual pulse structures, which are indicated by the heavy rectangular boxes, can be found. Clearly, the pulses, which stand on the same side of the peaks, are distinct from the kinks (or antikinks), which connect the two different sides. However, like the kinks, the pulses also get wider with increase of the coupling [compare Figs. 1(a)–1(d)], i.e., more lattices get into the disordered regions. In this paper, we refer to the particular localized coherent structure (kink or pulse) in space as an independent mode. Note that these two different mode patterns considered as two basic coherent structures, as illustrated in Fig. 2(a) for the kink (front) and Fig. 2(b) for the pulse, have been extensively studied in the pattern formation field [2].

Furthermore, to show the variation of the patterns versus ε clearly, we plot the bifurcation diagram in Fig. 3(a) and characterize the patterns with the maximum Lyapunov exponent $\lambda_{\max}$ in Fig. 3(b). The Lyapunov characteristic exponent [1] gives the rate of exponential divergence from perturbed initial conditions. The maximum Lyapunov exponent, the largest one in the Lyapunov characteristic exponent spectrum, is the most important one for characterizing the system's dynamics. Usually, if it is larger than zero, the system is chaotic, whereas if it is equal to or lower than zero, the system is regular. A standard numerical computational method for $\lambda_{\max}$ [15] with the linearization equations of Eq. (1) has been utilized. Unusual global patterns with a brush-

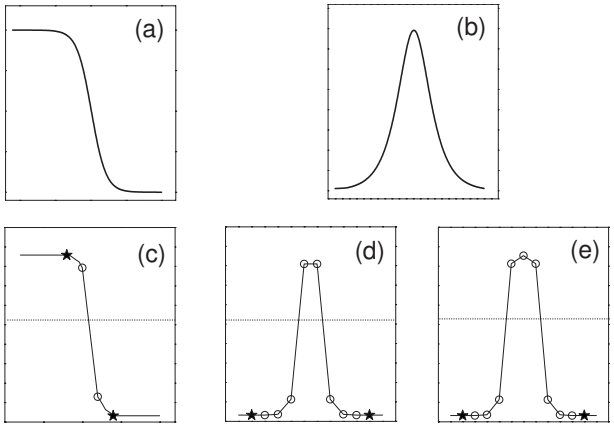

FIG. 2. (a), (b) Schematic illustrations for the kink (front) and the pulse, respectively. (c) (d) (e). Schematic diagrams of the modes for the kink pattern $M_k=2$, and the pulse patterns $M_p=2$ and 3, respectively. The unknown sites are denoted by open circles, while the fixed boundaries are denoted by stars.

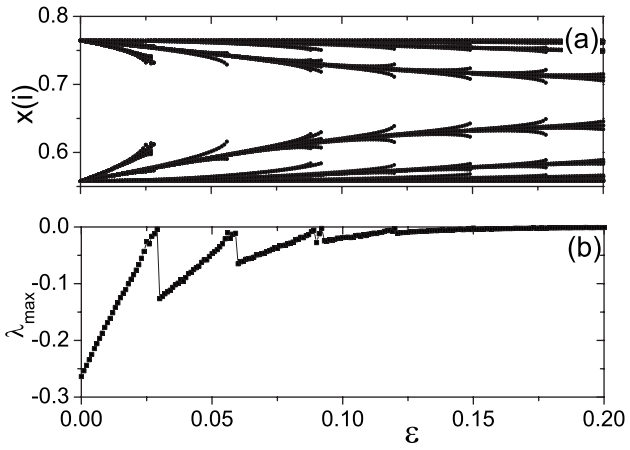

FIG. 3. (a) Bifurcation diagram of the coupled map lattice and (b) the maximum Lyapunov exponent of the CML λ_{max} vs ε.

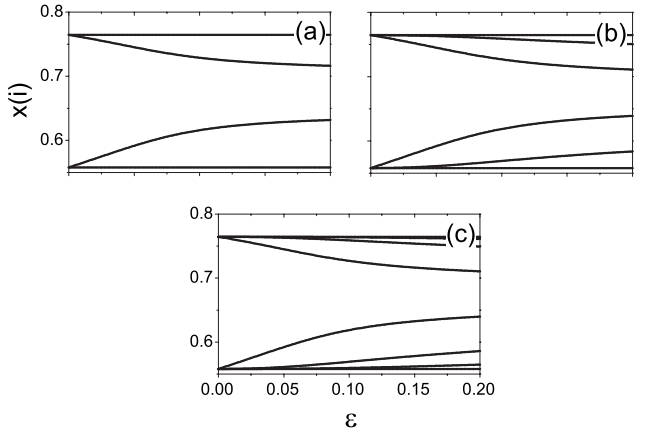

FIG. 4. (a), (b), (c) Bifurcation diagrams of the kink from the mode analysis for the different mode numbers M_k=2, 4, and 6, respectively.

like bifurcation structure and a zigzag Lyapunov exponent form are discernible. Roughly, the disordered brushlike curves (branches) originate and bifurcate from the several main unbroken curves (stems), and break at certain couplings, whose values correspond to the zero-crossing transition points of λ_{max}. We should note that the roughly equal distance between these critical coupling parameters is a coincidence for this particular parameter μ=3.1 only. All these observations are regarded as significant and need a theoretical explanation.

III. THE MODE ANALYSIS

Let us consider the patterns in Fig. 1 and focus our attention on the detailed mode structure of the isolated kinks and pulses. As both the kinks and the pulses are well separated by the flat regions, we might be able to cut them from the whole system. We schematically show the isolated mode structures for the mode of the kink (M_k=2) in Fig. 2(c). Due to the symmetry, only even modes for the kink are possible. Here the mode number M_k corresponds to the number of lattices moving into the middle region of the kink mode. For example, for M_k=2, shown in Fig. 2(c), there are only two lattices (indicated with the open circles), whose positions are within x_1^* and x_2^*, surrounded by the two boundary lattices fixed to x_1^* and x_2^* (denoted by the stars). This mode could approximately describe the kink structure that is highlighted by the thin box in Fig. 1(a). Similarly, we schematically show the even mode of the pulse (M_p=2) and the odd mode of the pulse (M_p=3) in Figs. 2(c) and 2(d), respectively. Here M_p represents the number of lattices above x^* in the mode distribution. The single mode of the pulse having three lattices (points) above x^* in M_p=3, illustrated in Fig. 2(e), is a good approximation to the structure emphasized with the heavy box in Fig. 1(b). Thus, with the above notation, (M_k=2, M_p=2), (M_k=4, M_p=3), (M_k=6, M_p=6), and (M_k=6, M_p=7) could represent the isolated modes for the kinks and the pulses in Figs. 1(a)–1(d), respectively.

One may ask, can we predict these modes, or, in particular, obtain the specific locations of these lattices? The answer is yes. One reason is that now in the mode approximation the two boundaries of the kink are fixed at x_1^* and x_2^*, the two boundaries of the pulse are fixed to x_1^*, and both the kinks and pulses have been well cut out from the whole coupled system. The other reason is that the unknowns (the positions of the lattices within the mode) will asymptote to the stable solutions in the isolated mode equations for proper initial settings for these unknowns. From the original coupling equations [Eq. (1)] the coupled equations for the M_k mode read

$$x_{n+1}(1) = f(x_n(1)),$$

$$x_{n+1}(i) = (1-\varepsilon)f(x_n(i)) + \frac{\varepsilon}{2}[f(x_n(i-1)) + f(x_n(i+1))],$$

$$i = 2, \ldots, N-1,$$

$$x_{n+1}(N) = f(x_n(N)), \tag{2}$$

with the two boundary lattices fixed to $x_0(1)=x_1^*$ and $x_0(N)=x_2^*$ for the kink mode. $N=M_k+2$ and M_k is even. The numerical results of the bifurcation diagrams for M_k=2, 4, and 6 are presented in Figs. 4(a)–4(c), respectively, where we can see how the mode structure changes with the coupling strength. For convenience, in solving the equations we consider the symmetry of the mode. The different branches in each panel indicate the solution branches for the different lattices of the corresponding mode. Clearly, the number of branches in Fig. 4 becomes larger for larger M_k; there are M_k+2 branches for the M_k kink mode. Two trivial branches for x_1^* and x_2^* (the top and the bottom horizontal lines) are always solutions of the equations. We also find that for the M_k=6 mode the number of branches splits from 2 to 4 at $\varepsilon \approx 0.05$, and from 4 to 6 at $\varepsilon \approx 0.12$. This finding is consistent with our previous observation that the width of the kink gets larger with increase in the coupling and more lattices move into the middle kink regions. For small coupling, the higher modes degenerate into the low modes (compare the curves in

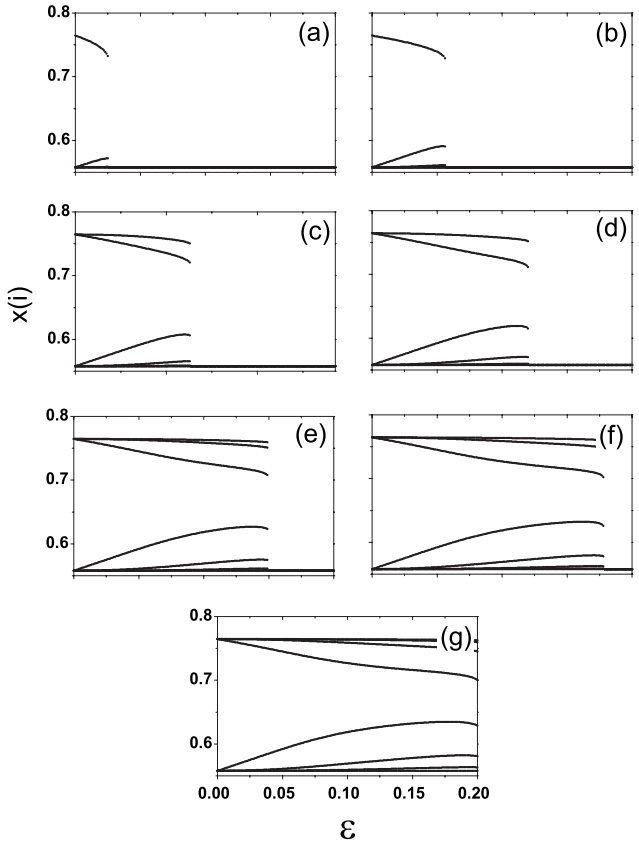

FIG. 5. (a)–(g) The same as Fig. 4 for the pulse number M_p from 1 to 7.

Fig. 4). Thus we need to consider only the $M_k=6$ mode in the parameter regime $0 \leq \varepsilon \leq 0.2$ studied here.

Similarly, we solve the mode equations for the pulse with the same form as Eqs. (2) but with the two boundary lattices fixed to $x_0(1)=x_1^*$ and $x_0(N)=x_1^*$ and N being sufficiently large ($N \gg M_p$). In simulations, a special initial condition for the M_p mode should be used: the initial values for the middle M_p lattices have to be set larger than x^* and the others lower than x^*. In solving the equations we consider the symmetry of the mode again. We plot the bifurcation diagrams for each mode of the pulse from $M_p=1$ to 7 in Fig. 5. Clearly, the number of branches also gets larger for larger M_p as more lattices move into the middle pulse regions; in particular, there are $(M_p+1)/2$ branches above x^* for the odd M_p (or $M_p/2$ branches for the even M_p) owing to symmetry [see Figs. 2(d) and 2(e) for the schematic definition of the pulse mode]. Unlike the splitting behavior of the bifurcation curves of the modes of the kink, the bifurcation curves of the modes of the pulse become broken step by step from low to high mode number. The transition parameters for the modes from 1 to 7 are $\varepsilon \approx 0.029$, 0.059, 0.092, 0.120, 0.151, 0.178, and 0.204, respectively. The mechanism for this instability will be investigated below.

We plot all the bifurcation diagrams of $M_k=6$ [Fig. 4(c)] and M_p from 1 to 7 (Fig. 5) in Fig. 6(a). All of the other branches at the next time step have been added. Clearly, the pattern is similar to the original bifurcation diagram for all lattices [Fig. 3(a)]. We also calculate the maximum

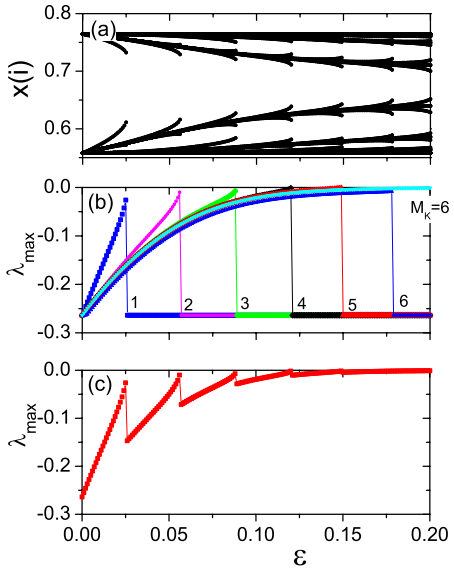

FIG. 6. (Color online) (a) Bifurcation diagram of the model for the kink and pulse patterns for all modes $M_k=6$ and M_p (from 1 to 7). (b) Maximum Lyapunov exponents (MLEs) of the pulses for each mode M_p (from 1 to 6) and the kink $M_k=6$ vs ε. (c) The largest value of the MLEs for all the kink and pulse modes obtained in (b) vs ε.

Lyapunov exponent for each mode with the same standard numerical method [15] but this time with the reference orbit of the mode equations [Eqs. (2)]. The results are shown in Fig. 6(b). The largest values at fixed ε for each mode are chosen and plotted in Fig. 6(c), which is largely similar to the λ_{max} of the coupled systems in Fig. 3(b). We would like to emphasize that our mode analysis theory is only an approximation theory, which in principle allows us to cut *isolated* spatial structures (kinks or pulses) surrounded by flat regions from the whole coupled system for an independent analysis. Thus, although the main theoretical results are attractive, the predicted values for the thresholds of λ_{max} appear a little earlier than the real values [comparing Fig. 6(c) with Fig. 3(b)].

Our mode analysis method not only catches the global feature of the patterns, as shown in the bifurcation figure and the maximum Lyapunov exponent plot in Fig. 5, but also predicts the detailed structure for the lattices, given the spatial position and the mode number of the specific mode. For instance, the modes in the boxes in Fig. 1 have been well predicted, as exemplified in Fig. 7 (comparing the left and right columns).

One final question still needs to be answered: What is the underlying mechanism for the instability of the pulse mode, or what kind of bifurcation is supposed to happen when the maximum Lyapunov exponent reaches zero? From the bifurcation diagrams of the pulse modes, we know that the high lattices get lower and the low lattices get higher with increase of the coupling, and then the pulse mode becomes unstable and disappears completely as the critical coupling parameter is touched [see, for example, Fig. 5(a)]. Thus, a tangent bifurcation is expected. To check this point, a numerical experiment is performed by using the Newton-

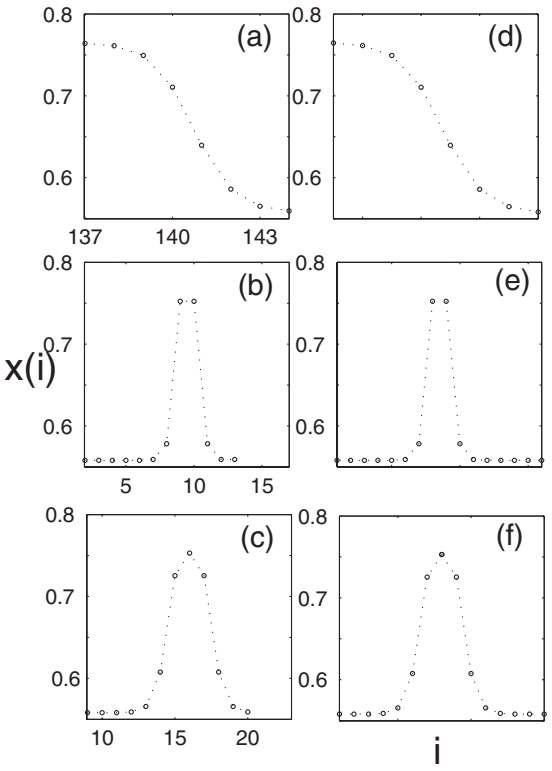

FIG. 7. Left column: (a), (b), (c) Enlargements of the thin box in Fig. 1(d), the heavy box in Fig. 1(a), and the heavy box in Fig. 1(b), respectively. Right column: (d), (e), (f) Theoretical predictions of the modes $M_k=6$, $M_p=2$, and $M_p=3$, respectively.

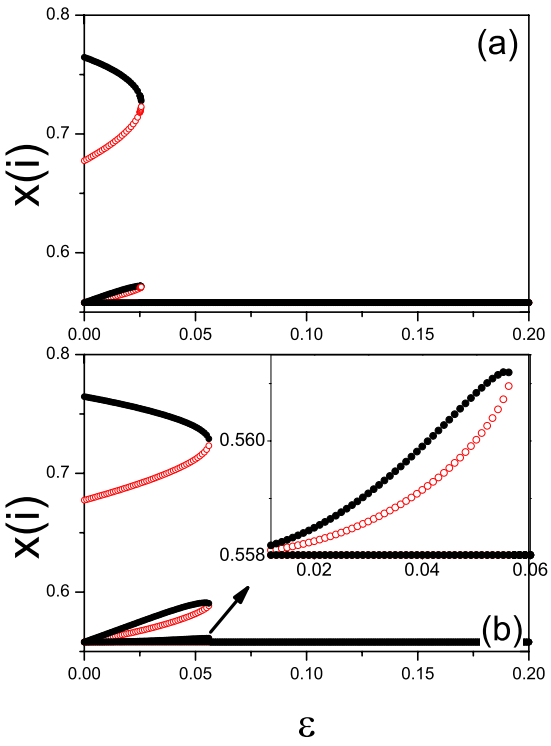

FIG. 8. (Color online) (a), (b) The same as Fig. 5 for the pulse numbers $M_p=1$ and 2, respectively, with the Newton-Raphson algorithm used instead. The solid (open) dots represent the stable (unstable) solutions. Clearly, the stable and unstable solution branches collide and both are annihilated at the instability coupling parameter, reflecting the tangent bifurcation nature. The inset in (b) is the enlargement of the left lower part of the two stable and unstable branches.

Raphson algorithm [16] to find the solutions of the pulse mode equations [Eqs. (2)]. Unlike the usual brute-force approach, which can get a stable solution only and has been used in Figs. 4 and 5, the Newton-Raphson approach can locate stable and unstable limit sets. The results are shown in Figs. 8(a) and 8(b) for $M_p=1$ and 2, respectively. The stable solutions, which are the same as those in the bifurcation diagrams in Fig. 5, are denoted by the solid points, and the newly found unstable solutions are denoted by the open ones. Remarkably, the stable branches of the pulse collide with the unstable branches at the critical parameter, and the whole stable pulse mode is annihilated. Therefore, the destructive nature of the pulse mode through the tangent bifurcation has been verified. The unstable solution obtained has a structure that is quite different from that of the corresponding stable solution. One clear observation is that the stable pulse solution starts from the x_1^* (or x_2^*) point at $\varepsilon=0$, whereas one of the middle unstable pulse solution curves starts from the x^* point. It is notable that, apart from the unstable branches plotted in Fig. 8, several other unstable solutions have been obtained from the simulations for different initial condition settings, which are not included in the figure and have no significant contribution to the instability of the mode. Thus, now it is easy to understand the unusual brushlike bifurcation diagram and the zigzag Lyapunov exponent pattern in Fig. 3, and the significant but distinct roles of the kink and pulse modes in the organization of the patterns: the effect of the kink is modest, but that of the pulse is severe.

We can easily extend the above analysis of the period-2 case to higher-period cases. For example, Fig. 9(a) shows a period-4 pattern at one time instant at $\mu=3.5$ and $\varepsilon=0.3$. Clearly, both kinks and pulses of different modes, highlighted with the boxes, are visible, although this time the situation becomes more complicated with four possible subbranches (boundaries) in which the kinks and the pulses can be chosen. Figure 9(b) displays the bifurcation diagram of the coupled systems [Eq. (1)], and for comparison Fig. 9(c) plots our theoretical prediction result after we carefully analyzed all the possible modes by the mode analysis method. Again they are in good agreement.

IV. CONCLUSION AND BRIEF DISCUSSION

In conclusion, we have studied the period doubling of kink-antikink patterns in coupled map lattices. This type of pattern is simple but complex; it takes place immediately after the period-doubling bifurcation of the map. On the basis of the mode analysis, the common features of the patterns constructed by the three distinct modes, including the kink, the pulse, and the flat, have been well uncovered. The self-organization, the evolution process, and the bifurcation behavior have been revealed. To conclude, the dynamics of the complex patterns in periodic regimes with both kinks and

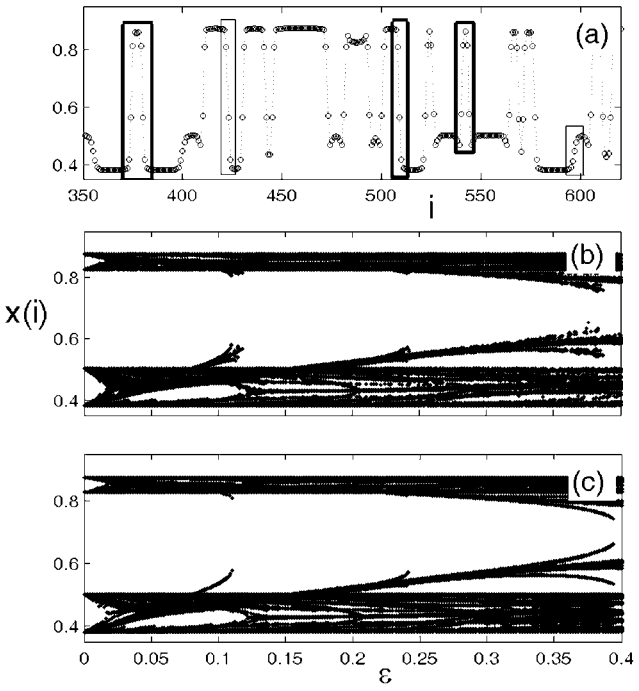

FIG. 9. (a) Snapshot of the coupled map lattices at $\mu=3.5$ within the period-4 regime and $\varepsilon=0.3$. The kink and pulse modes are emphasized with the boxes. (b) Bifurcation diagram of the CML and (c) the prediction from the mode analysis.

pulses has been well described with the help of our mode analysis.

Finally, it is worthwhile to give some brief discussion. First, except for the kink and pulse solutions discussed in the paper, there exist some stable solutions to the mode equations [Eqs. (2)] which have not been considered. For instance, there exist similar kink solutions with odd numbers of oscillators with the middle point being on the fixed $P1$ solution under sufficiently large coupling. Nevertheless, in coupled systems, a small perturbation might shift the above-mentioned odd-number kink mode to the more stable even-number kink mode, which actually makes the odd-number kinks unobservable; this point has been confirmed by the observation of the pattern distributions in Fig. 1. Second, we have also tested the cases where the coupled logistic maps are nonidentical with small amounts of random parameter mismatch [e.g., the μ_i's have been varied within $(\mu-\Delta\mu,\ \mu+\Delta\mu)$, $\mu=3.1$ and $\Delta\mu=0.005$], and the global patterns with kinks and pulses persist. Thus, the observations with respect to the isolated mode structure appear to be robust for small parameter disturbances. Third, we admit that the mode analysis method has been developed in different circumstances for completely different problems, such as the analysis of a periodic window in weakly coupled map lattices [9] and the study of generalized splay states induced by weak mutual resonant interactions in coupled chaotic flow systems [17,18]. In these two cases, only a single mode with three coupled nonlinear elements at extremely weak coupling has been discussed. Fourth, we would like to emphasize that, although our study appears to be a simple model study, it has the potential to impact numerous other systems. In particular, the analytical method could be beneficial. For example, in two-dimensional complex oscillatory chemical systems described by a partial differential equation, the global period-2 spiral waves with a locally period-1 defect line [19,20] have some qualitative features quite similar to the kink-pulse pattern studied here. The studies not only will attract general interest from researchers in the fields of spatiotemporal chaos and pattern dynamics, but also have many potential applications in the fields of biology, ecology, chemistry, mathematics, and engineering.

ACKNOWLEDGMENTS

This work was partially supported by the Foundation of Wuhan Institute of Physics and Mathematics under Grant No. T06S607, and the National Natural Science Foundation of China under Grants No. 10575016 and No. 10675161. The authors thank Dr. B. S. V. Patnaik for his comments and help. We also express our thanks to both anonymous referees for constructive comments and criticisms.

[1] E. Ott, *Chaos in Dynamical Systems* (Cambridge University Press, New York, 1993), and references therein; Bai-lin Hao, *Starting with Parabolas—An Introduction to Chaotic Dynamics* (Shanghai Scientific and Technological Education Publishing House, Shanghai, 1993) (in Chinese).
[2] M. C. Cross and P. C. Hohenberg, Rev. Mod. Phys. **65**, 851 (1993).
[3] K. Kaneko, *Theory and Applications of Coupled Map Lattices* (Wiley, New York, 1993).
[4] J. P. Cruthfield and K. Kaneko, in *Directions in Chaos*, edited by H. Bai-lin (World Scientific, Singapore, 1987), p. 272.
[5] K. Kaneko, Physica D **34**, 1 (1989).
[6] K. Kaneko, Physica D **37**, 60 (1989).
[7] Chaos **2**, 279 (1992), focus issue on coupled map lattices in chaos, edited by K. Kaneko.
[8] K. Kaneko, Prog. Theor. Phys. **72**, 480 (1984).
[9] E. J. Ding and Y. N. Lu, J. Phys. A **25**, 2897 (1992).
[10] F. H. Willeboordse, Phys. Lett. A **183**, 187 (1993).
[11] F. H. Willeboordse, Phys. Rev. E **65**, 026202 (2002).
[12] F. H. Willeboordse, Phys. Rev. Lett. **96**, 018702 (2006).
[13] R. M. May, Nature (London) **261**, 459 (1976).
[14] M. J. Feigenbaum, J. Stat. Phys. **19**, 25 (1978); **21**, 669 (1979).
[15] A. Wolf, J. B. Swift, H. L. Swinney, and J. A. Vastano, Physica D **16**, 285 (1985).
[16] T. S. Parker and L. O. Chua, *Practical Numerical Algorithms*

for Chaotic Systems (Springer-Verlag, New York, 1989), Chap. 5.
[17] M. Zhan, G. Hu, Y. Zhang, and D. H. He, Phys. Rev. Lett. **86**, 1510 (2001).
[18] D. H. He, G. Hu, M. Zhan, and H. P. Lu, Physica D **156**, 314 (2001).
[19] A. Goryachev, H. Chate, and R. Kapral, Phys. Rev. Lett. **80**, 873 (1998).
[20] M. Zhan and R. Kapral, Phys. Rev. E **72**, 046221 (2005).